electronics

MDPI

Article

A New Single-Phase Direct Frequency Controller Having Reduced Switching Count without Zero-Crossing Detector for Induction Heating System

Naveed Ashraf [1], Tahir Izhar [1], Ghulam Abbas [2,*], Ahmed Bilal Awan [3], Ali S. Alghamdi [3,*], Ahmed G. Abo-Khalil [3], Khairy Sayed [4], Umar Farooq [5] and Valentina E. Balas [6]

1 Department of Electrical Engineering, University of Engineering and Technology, Lahore 54890, Pakistan; naveed.ashraf@ee.uol.edu.pk (N.A.); tizhar@gmail.com (T.I.)
2 Department of Electrical Engineering, The University of Lahore, Lahore 54000, Pakistan
3 Department of Electrical Engineering, Faculty of College of Engineering Majmaah University, Majmaah 11952, Saudi Arabia; a.awan@mu.edu.sa (A.B.A.); a.abokhalil@mu.edu.sa (A.G.A.-K.)
4 Faculty of Engineering, Sohag University, Sohag 82524, Egypt; khairy_fathy@yahoo.ca
5 Department of Electrical Engineering, University of the Punjab, Lahore 54590, Pakistan; engr.umarfarooq@yahoo.com
6 Department of Automatics and Applied Software, "Aurel Vlaicu" University of Arad, 310130 Arad, Romania; valentina.balas@uav.ro
* Correspondence: ghulam.abbas@ee.uol.edu.pk (G.A.); aalghamdi@mu.edu.sa (A.S.A.)

Received: 3 February 2020; Accepted: 26 February 2020; Published: 4 March 2020



Abstract: Induction heating (IH) is an environmentally friendly solution for heating and melting processes. The required high-frequency magnetic field is accomplished through frequency controllers. Direct frequency controllers (DFC) are preferred to dual converters as they have low conversion losses, compact size, and simple circuit arrangement due to low component count. Numerous frequency controllers with complex switching algorithms are employed in the induction heating process. They have a complicated circuit arrangement, and complex control as their switching sequences have to synchronize with source voltage that requires the zero-crossing detection of the input voltage. They also have a shoot-through problem and poor power quality. Therefore, this research proposes a novel frequency controller with a low count of six controlled switching devices without a zero-crossing detector (ZCD) having a simple control arrangement. The required switching signals are simply generated by using any pulse-width-modulated (PWM) generator. The performance of the proposed topology is verified through simulation results obtained using the MATLAB/Simulink environment and experimental setup.

Keywords: frequency controller; domestic induction heating; power quality; shoot-through problem; zero-crossing detector

1. Introduction

Nowadays, domestic and industrial induction heating is one of the hot research areas due to low conversion losses, low processing time, pollution-free operation, and accurate power control [1]. It is employed in many applications such as domestic induction heating (induction cooker, domestic induction appliances burners, etc.) [2–4], medical applications [5], and wireless power transfer [6]. Its basic operating principle is to apply a high-frequency magnetic field to the heating targets. The typical frequency range for these applications lies from 20 kHz to 100 kHz. The output frequency can be regulated through dual converters [7,8] and direct alternating current to alternating current (ac-to-ac) converters [9–13].

Conventionally, high-frequency IH systems are implemented in two conversion stages. The first stage involves rectification, where ac grid voltage is converted to dc voltage through the alternating current to direct current (ac-to-dc) converters. A low pass filter is required to reduce the ripple factor of the output voltage. The improvement in output ripple deteriorates the power quality of the input current. Many control techniques and switching algorithms are developed to improve the power quality by using feedback controllers such as fuzzy or sliding mode controllers, as reported in [14]. In the second conversion stage, the rectified output is converted to high-frequency ac voltage with the help of a resonant converter. Various topologies of resonant converters in the form of half-bridge and full-bridge series resonant inverters are developed [15–17] to obtain the required output voltage. In dual converters, an ac voltage is converted to variable ac voltage and frequency indirectly, so these converters are also known as indirect converters. But they are complex and have high conversion losses and high cost due to a large count of the switching devices.

Direct ac-to-ac converters are developed to overcome the demerits of the indirect ac-to-ac converters as they have a simple circuit arrangement, low conversion losses, and fewer switching devices. Ac voltage controllers regulate the output voltage both in buck and boost fashion [18–21]. They can be employed as frequency controllers if they have non-inverting and inverting characteristics [22–26]. These matrix converters regulate the output voltage through duty ratio control of the high-frequency switching devices. However, their switching sequences are complex and have high switching voltage and current stresses. The problem of high switching voltage is solved in [9,10] by using eight controlled switches, but they require complex switching sequences.

Complex switching algorithms and circuit complications are the major causes of less use of the single-phase matrix converters (SPMC) in induction heating applications. A direct ac-to-ac converter topology (see Figure 1) with a modified switching algorithm is developed in [27] to enhance the potency of SPMC for the induction heating application. It only requires two complementary pulse-width-modulated (PWM) signals to operate it as a resonant converter or direct frequency converter. These two control signals control the switching states of the eight semiconductor switching devices. Arduino Mega 2560 is employed to generate the gating signals, and these signals are synchronized with input ac voltage with the help of a zero-crossing detector (ZCD). Eight isolated dc power supplies with eight gate-driving circuits are required to switch the eight semiconductor switches of the dual bridge converter. An LC filter is used at the input side to suppress the unwanted harmonics to improve the input power factor. The topology suffers from the problem of the short-circuiting of the input capacitor of the switching transistor of each converter leg operated in a complementary fashion. Also, the zero-crossing detection of the input voltage in every cycle increases the control complexity.

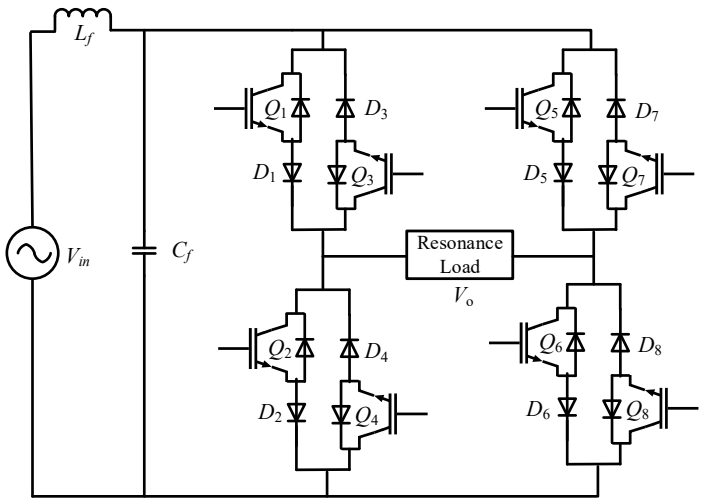


Figure 1. Direct alternating current to alternating current (ac-to-ac) resonance converter.

To overcome the aforementioned limitations of [27], this research develops a novel direct frequency changer for domestic induction heating applications having a low count of six switching devices and without a ZCD. The desired output frequency is obtained by operating the proposed converter in non-inverting and inverting modes. The proposed converter has no shoot-through problem. Therefore, there is no need to use the voltage snubber circuits for the protection of the high-frequency switching devices. Its operation only requires the generation of two high-frequency PWM switching signal in a complementary fashion. These signals can be generated with any PWM generator, as there is no need to detect the zero-crossing of the input voltage as switching frequency is kept much higher than that of the source as typical switching frequency lies in the range from 20 kHz to 100 kHz for domestic induction heating application. The control effort of the controller is reduced due to fewer numbers of the control signals and the absence of a zero-crossing detector. The six switching devices only require six isolated dc supplies and six gate-driving circuits. It reduces the two switching devices, two isolated dc supplies, two gate drive circuits, and one zero-crossing detector. Therefore, it reduces the overall size, cost, and conversion losses (thus improves conversion efficiency). Zero voltage switching of the switching devices is also ensured by selecting the switching frequency greater than the resonance frequency. The switching of high-frequency switches in a complementary fashion ensures the improved power factor and low total harmonic distortion (THD) of the input current. The hardware setup is developed to validate the simulation results obtained by modeling of the proposed converter in MATLAB/Simulink environment.

The paper is constructed in the following way. Section 2 demonstrates the circuit operation of all possible operating modes comprehensively. The performance of the proposed converter, in terms of components count, is computed and compared with the existing converters in Section 3. Section 4 involves the simulation and practical results to validate the effectiveness of the proposed converter system. The conclusion is drawn in Section 5.

2. Operation of the Proposed Topology

Figure 2a,b depicts the block diagram and the circuit topology of the suggested converter with gating signals. The operation of the proposed converter operating as a direct frequency changer (DFC) is divided into non-inverting and inverting modes. The controlled switching devices S_1, S_3, S_5 and S_2, S_4, S_6 are controlled in a complementary fashion with gating signal x_1 and x_2, respectively. There may be an open circuit problem of the inductor current due to switching of the controlled devices in a complementary way. This issue is tackled by inserting the small turn-off delay (T_{off}) in the switching signals (x_1 and x_2), as depicted in Figure 3, where T_c and T_p are the non-shoot through and the total conduction time of the switching devices, respectively. The switching and inductor currents are easily commutated from one switching pair to another as the proposed topology is free from the current shoot-through problem.

The control signals are directly generated with the PWM generator. There is no need to use ZCD to synchronize with input ac voltage as diode D_5, and D_6 only conducts for positive and negative half cycles of the input voltage, respectively. The gate drive circuits isolate the low voltage switching signals V_{g1} and V_{g2} from the high voltage of DCF. The R_o, L_o, and C_o represent the resistance, inductance, and capacitance of the heating load, respectively. The output frequency is governed by operating the proposed topology in the inverting and noninverting modes with almost a unity voltage gain, ensuring equal rms output and input voltage (see Figure 4).

The detail of each operating mode of the proposed converter is explored in Figure 5 with the help of switching states and highlighted paths of power transfer from input to output.

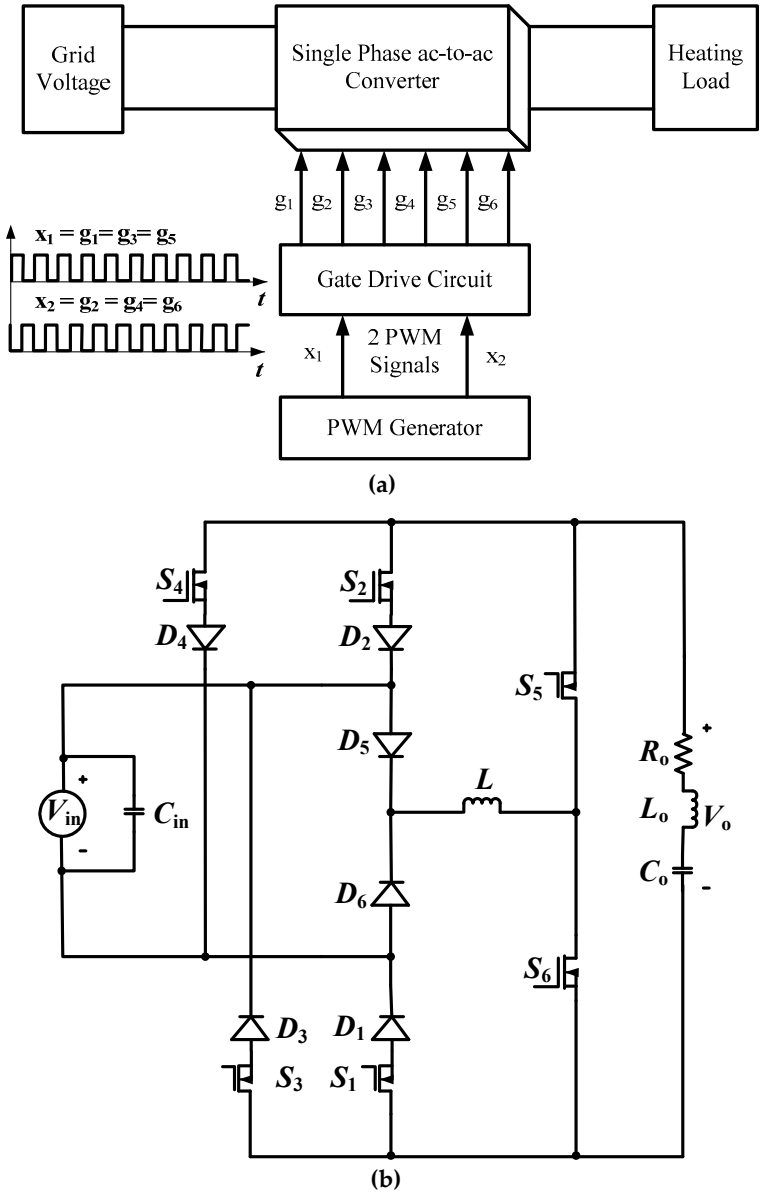


Figure 2. (**a**) Block diagram; (**b**) suggested converter.

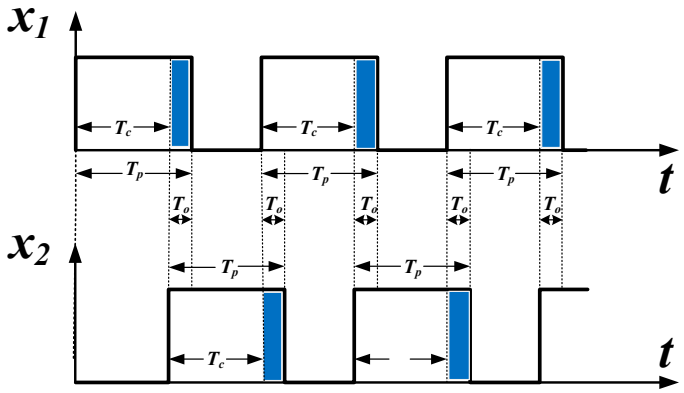


Figure 3. Turn-off delay in the switching signals.

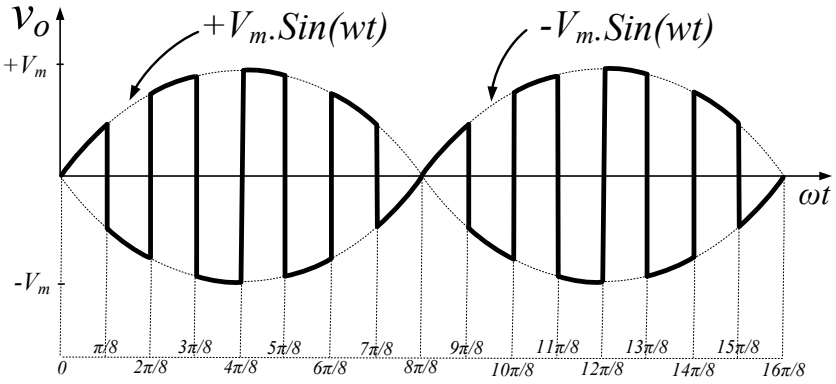


Figure 4. Voltage waveform for 400 Hz output frequency.

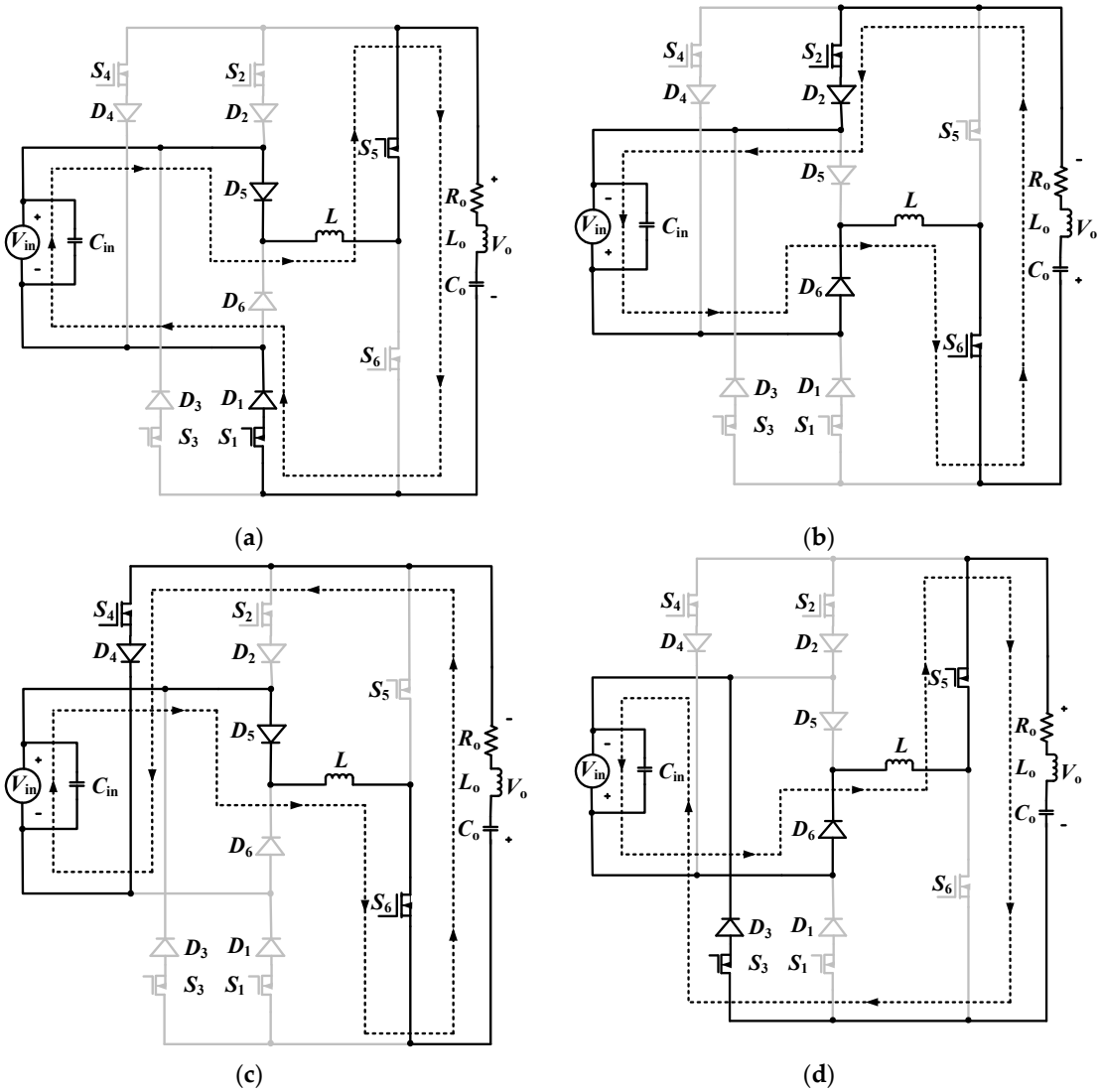


Figure 5. (**a**) and (**b**) non-inverting operation, (**c**) and (**d**) inverting operation.

2.1. Non-Inverting Operation

The operation of the proposed converter in this operating mode has positive voltage gain if the controlled switches S_1, S_3, S_5 and S_2, S_4, S_6 are switched in positive and negative half cycles of the source voltage, respectively. In the positive half cycle, the diodes D_5, D_1 are on, and D_2, D_3, D_4, D_6 are

off. The turned-on switch S_3 cannot conduct as its series-connected diode D_3 is reverse biased. In this interval, the load is connected to the input, as shown in the highlighted paths of Figure 5a. During the negative half cycle of the source voltage, the diodes D_2, D_6 become forward and D_1, D_3, D_4, D_5 reverse biased. The switch S_4 remains off in this interval due to reverse biasing of its series-connected diode D_4. The power flow path during this interval is exposed in Figure 5b. In this operation, the role of the switching devices is only to connect the load with the source. Therefore, the instantaneous value of the load voltage is equal to the input voltage. The dynamic state behavior of the inductor voltage for positive and negative input during non-inverting operation can be realized in Equation (1) to find out the voltage transfer ratio, as reported in [19].

$$L\frac{di}{dt} = v_{in} - 2i_o(R_{df} + R_{mf}) - 2V_{df} - v_o \tag{1}$$

where v_{in}, v_o, L, i_o, V_{df}, R_{df}, and R_{mf} are the instantaneous input voltage, output voltage, filtering inductor, instantaneous output current, diode forward voltage, and the internal resistances of the diode and the MOSFET, respectively. In steady-state condition, the relationship between the instantaneous value of the input and output voltage is developed in Equation (2) by ignoring the voltage drops in the internal resistances of the switching devices.

$$v_o = v_{in} \tag{2}$$

These results can also be formulated using the inductor volt-second product principle. The inductor voltage during the turn-off delay time (shoot-through time) is realized as:

$$v_L = T_o v_{in} \tag{3}$$

Similarly, the inductor voltage during the non-shoot through interval (T_c) is computed as:

$$v_L = T_c(v_{in} - v_o) \tag{4}$$

The average inductor voltage during one conduction interval is calculated as:

$$\frac{v_{in}T_o + (v_{in} - v_o)T_c}{T_p} = 0 \tag{5}$$

Or

$$\frac{v_o}{v_{in}} = \frac{T_c + T_o}{T_c} = B \tag{6}$$

where 'B' is the voltage boost factor or voltage transfer ratio. Equation (6) reduces to Equation (2) for the low value of shoot-through interval (T_o).

2.2. Inverting Operation

The switching of the controlled switching devices S_2, S_4, S_6, and S_1, S_3, S_5 ensure the negative voltage gain for positive and negative input voltage, respectively. The polarity of the input voltage determines the switching states of the diodes. The diodes D_5, D_4 become forward biased and D_1, D_2, D_3, D_6 reverse biased for positive input voltage. The reverse biasing of the diode D_2 forces the controlled switch S_2 to remain off in the non-conducting state. The output voltage is inverted with respect to source voltage, as can be observed from the power flow path of Figure 5c. The negative polarity of the source voltage forces the operation of diodes D_3, D_6 in the conduction state and D_1, D_2, D_4, D_5 in the off state. The controlled switch S_3 is not in conduction state due to reverse biasing of its series-connected diode D_3. The power flow path of Figure 5d depicts the inverted load voltage with

the negative input voltage. The inverting behavior of the output can also be further explored through the dynamic inductor voltage as depicted in Equation (7) for positive and negative input voltage.

$$L\frac{di}{dt} = v_{in} - 2i_o(R_{df} + R_{mf}) - 2V_{df} + v_o \tag{7}$$

Equation (7) is simplified by neglecting the internal voltage drops to have the voltage transfer ratio for inverting operation with any polarity of the input voltage. This is depicted in Equation (8):

$$v_o = -v_{in} \tag{8}$$

Similarly, the inductor voltage for the inverting operation during the short-through and non-short through intervals is computed respectively as:

$$v_L = T_o v_{in} \tag{9}$$

$$v_L = T_c(v_{in} + v_o) \tag{10}$$

The boost factor or the voltage transfer ratio during the inverting operation can be realized by computing the average value of the inductor voltage during its conducting interval as:

$$\frac{v_o}{v_{in}} = -\frac{T_c + T_o}{T_c} = -B \tag{11}$$

By ignoring the shoot-through interval, the boost factor becomes unity. So, the instantaneous value of the output voltage becomes equal to and opposite to the instantaneous value of the input voltage during the non-inverting and inverting operation, respectively. Therefore, the rms value of the output voltage is nearly equal to that of the input voltage as there are low voltage drops in the filtering inductor and switching devices. This is also explored analytically by computing the rms value of the output voltage at 400 Hz (see Figure 4).

This output is generated by operating the proposed topology alternatively eight times in non-inverting and inverting mode. The rms output voltage is simply computed as:

$$\begin{aligned} V_{o(rms)} &= \sqrt{\begin{aligned} &\tfrac{2}{2\pi}\int_{0}^{\pi/8}\left(+V_m^2\right)\sin(\omega t)^2 d(\omega t) + \tfrac{2}{2\pi}\int_{\pi/8}^{2\pi/8}\left(-V_m^2\right)\sin(\omega t)^2 d(\omega t) \\ &+\tfrac{2}{2\pi}\int_{2\pi/8}^{3\pi/8}\left(+V_m^2\right)\sin(\omega t)^2 d(\omega t) + \tfrac{2}{2\pi}\int_{3\pi/8}^{4\pi/8}\left(-V_m^2\right)\sin(\omega t)^2 d(\omega t) \\ &+\tfrac{2}{2\pi}\int_{4\pi/8}^{5\pi/8}\left(+V_m^2\right)\sin(\omega t)^2 d(\omega t) + \tfrac{2}{2\pi}\int_{5\pi/8}^{6\pi/8}\left(-V_m^2\right)\sin(\omega t)^2 d(\omega t) \\ &+\tfrac{2}{2\pi}\int_{6\pi/8}^{7\pi/8}\left(+V_m^2\right)\sin(\omega t)^2 d(\omega t) + \tfrac{2}{2\pi}\int_{7\pi/8}^{8\pi/8}\left(-V_m^2\right)\sin(\omega t)^2 d(\omega t) \end{aligned}} \\ &= \frac{V_m}{\sqrt{2}} \end{aligned} \tag{12}$$

Therefore,

$$V_o(rms) = V_{in}(rms) = 106\ V, \text{ for 150 peak input voltage} \tag{13}$$

The details of the switching states of the semiconductor switching devices in each operating interval are also explored in Table 1.

Table 1. The switching states of the semiconductor devices during non-inverting and inverting operation.

Non-Inverting Operation								**Inverting Operation**							
$V_{in} > 0$				$V_{in} < 0$				$V_{in} > 0$				$V_{in} < 0$			
S_1	on	D_1	on	S_1	off	D_1	off	S_1	off	D_1	on	S_1	on	D_1	off
S_2	off	D_2	off	S_2	on	D_2	on	S_2	on	D_2	off	S_2	off	D_2	on
S_3	on	D_3	off	S_3	off	D_3	on	S_3	off	D_3	off	S_3	on	D_3	on
S_4	off	D_4	on	S_4	on	D_4	off	S_4	on	D_4	on	S_4	off	D_4	on
S_5	on	D_5	on	S_5	off	D_5	off	S_5	off	D_5	on	S_5	on	D_5	off
S_6	off	D_6	off	S_6	on	D_6	on	S_6	on	D_6	off	S_6	off	D_6	on

It is clear from Figure 5 and Table 1 that in each operating interval, only two controlled switches and two diodes are in conducting states.

3. Performance Evaluation and Comparison

The non-inverting and inverting operation of the proposed converter and converter in [27] is achieved with high-frequency PWM control of two switches and two diodes. Therefore, they have the same switching and conduction losses. As the switching frequency is very high compared to the output frequency, the switching voltages and currents are assumed quasi dc. The average switching losses of a MOSFET and diode are computed in Equations (14) and (15), respectively, as discussed in reference [28].

$$P_{sw(MOSFET)} = \frac{f_{sw}}{2}\left\{\left(I_{sw}V_{sw}(t_r + t_f\right) + C_oV_{sw}^2\right\} \tag{14}$$

$$P_{sw(diode)} = f_{sw}Q_{RR}V_{sw} \tag{15}$$

As each MOSFET and diode conducts for the half period of the input voltage, so their average switching power in the period of the input voltage is realized in Equations (16) and (17), respectively.

$$P_{sw(MOSFET)} = \frac{f_{sw}}{4}\left\{\left(I_{sw}V_{sw}(t_r + t_f\right) + C_oV_{sw}^2\right\} \tag{16}$$

$$P_{sw(diode)} = \frac{1}{2}f_{sw}Q_{RR}V_{sw} \tag{17}$$

In one cycle of the input voltage, four diodes and four MOSFETs operate to realize the high-frequency output voltage, so the total switching power losses in one cycle of the input voltage are formulated in Equation (18).

$$P_{sw} = f_{sw}\left[\left\{\left(I_{sw}V_{sw}(t_r + t_f\right) + C_oV_{sw}^2\right\} + 2Q_{RR}V_{sw}\right] \tag{18}$$

The duty cycle of each conducting device is 50%. The average conduction losses of a MOSFET and diode in one cycle of the input voltage are formulated in Equations (19) and (20), respectively.

$$P_{cond(MOSFET)} = \frac{1}{4}I_{sw}^2R_{mf} \tag{19}$$

$$P_{cond(diode)} = \frac{I_{sw}}{4}\left(V_{df} + I_{sw}R_{df}\right) \tag{20}$$

The total conduction losses during the one cycle of the input are the sum of the conduction losses of the four MOSFETs and four diodes, and they are computed as in Equation (21).

$$P_{cond} = I_{sw}\left\{V_{df} + I_{sw}\left(R_{mf} + R_{df}\right)\right\} \tag{21}$$

where f_{sw}, I_{sw}, V_{sw}, C_o, t_r, t_f, and Q_{RR} are the switching frequency, switching current, switching voltage, on-state resistance, output capacitance, rise and fall times of the MOSFET, forward voltage, forward resistance and reverse recovery charge of the fast recovery diode, respectively.

The converter in [27] is implemented with a dual full-bridge converter, which has two extra fast recovery diodes and two MOSFETs than that of the proposed converter. The suggested research eliminates the use of two extra controlled switches and diodes. This ensures the reduction in losses and cost of the two gate drives circuits and two isolated dc supplies as switching of each transistor requires one isolated dc supply and gate drive circuit. As there is no need to synchronize the input voltage with gating signals, so it eliminates the use of ZCD as well. The control signals may be generated with any PWM generator. Hence these characteristics of the proposed converter decrease the size, cost, and control complexity significantly.

The converters in [23,29] are introduced to have variable output voltage and frequency. The converter in [29] employs the z-source arrangements to solve the shoot-through problem and to have a wide range of voltage gain. But this solution increases the size and cost as it requires extra passive components and switching devices. The large count of the passive components and switching devices are eliminated in [23]. The converters in [23,29] operate well once their output frequency requirement is less than the few kHz. But for high-frequency operation, their switching sequence becomes complicated. Their operation requires the conduction of three transistors and diode in any switching PWM interval. The proposed converter employs a simple switching algorithm that is effectively employed in the low- and high-frequency operation. They also have the problem of high switching voltage and currents that increase the conversion losses.

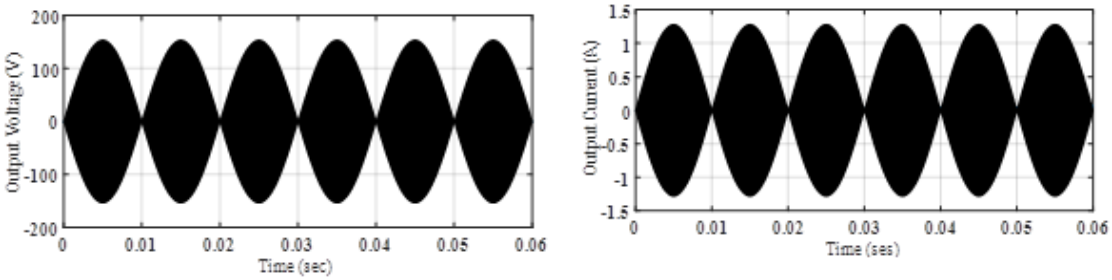
The detail of the comparison of the proposed topology with the converters in [23,27,29] in terms of components count and performance characteristics is tabulated in Table 2.

Table 2. Comparison with the existing converters in terms of components count and performance characteristics.

Components	**The Proposed Converter**	**The Converter in [23]**	**The Converter in [27]**	**The Converter in [29]**
Number of Transistors	6	6	8	10
Number of Diodes	6	6	8	10
Number of Filtering Capacitors	2	2	2	4
Number of Filtering Inductors	1	1	1	4
Number of Gate Drives Circuits	6	6	8	10
Number of Isolated DC Supplies	6	6	8	10
Number of ZCDs	0	1	1	1
Number of Conducting Devices at Any Time Instant	2 Transistors, 2 Diodes	3 Transistors, 3 Diodes	2 Transistors, 2 Diodes	3 Transistors, 3 Diodes
Voltage Gain Characteristics	Continuous Unity	Continuous Unity	Continuous Buck-boost	Discontinuous Buck-boost
Output Frequency Characteristics	Step Change	Step Change	Step Change	Step Change
Switching Current at Unity Voltage Gain	I_o	I_o	$2I_o$	I_o
Switching Voltage at Unity Voltage Gain	V_{in}	V_{in}	$2V_{in}$	V_{in}
Conduction Losses at Unity Voltage Gain	$I_oV_{df}+I_o^2\left(R_{mf}+R_{df}\right)$	$I_oV_{df}+I_o^2\left(R_{mf}+R_{df}\right)$	$3I_oV_{df}+4I_o^2\left(R_{mf}+R_{df}\right)$	$1.5I_oV_{df}+1.5I_o^2\left(R_{mf}+R_{df}\right)$
Open Circuit Problem	No	No	No	No
Shoot Through Problem	No	No	No	No

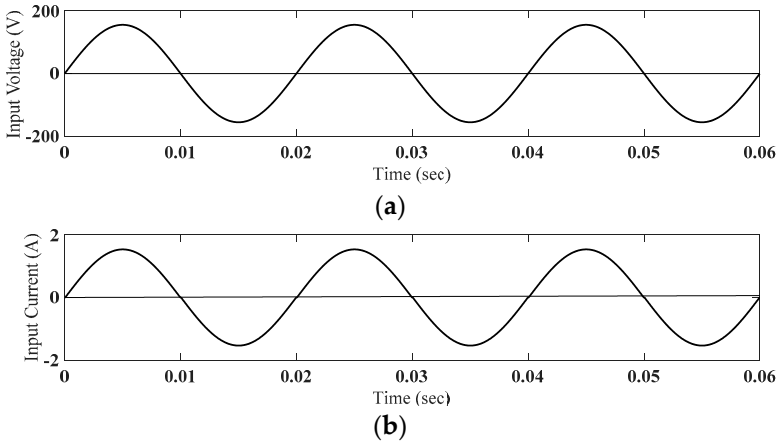
4. Simulation and Practical Results

The MATLAB/Simulink environment is used to explore the proposed topology. In this implementation, the input voltage is considered to be 150 V peak value at a frequency of 50 Hz. The switching frequency of the gating sequences is set to 25 kHz. The simulation waveforms of the output voltage and current are shown in Figure 6a,b, respectively. The output voltage and current are non-inverted and inverted both in the positive and negative half period of the input voltage at a switching frequency of 25 kHz. Similarly, the waveform of the input current with respect to the input voltage is shown in Figure 7, ensuring the high input power factor.



(**a**) (**b**)

Figure 6. Simulation waveforms of (**a**) output voltage and (**b**) output current.



(**a**)

(**b**)

Figure 7. Simulation waveforms of (**a**) input voltage and (**b**) input current.

The power quality of the input current is explored by taking its fast Fourier transform (FFT) in MATLAB/Simulink environment, and its total harmonic distortion (THD) is found to be less than 5% as shown in Figure 8. This is due to its continuous nature as it is conducted by D_1, D_5, S_1, S_5 and D_2, D_6, S_2, S_6 during the positive half cycle and the negative half cycle of the input voltage respectively for non-inverting mode. Similarly, the conduction of D_4, D_5, S_4, S_6 and D_3, D_6, S_3, S_5 during positive and negative half periods of the source voltage respectively ensures its continuous conduction in inverting operation.

A practical prototype is also developed to validate the elimination of ZCD and the attained simulation results. It consists of six controlled switches (IRF840), six fast recovery diodes (RHRG3040), and one input inductor and capacitor of 1 mH and 1 µF, respectively. The six gate driving circuits are employed with hybrid chips (EXB840) with six isolated dc supplies. Figure 9 shows the hardware implementation of the proposed converter.

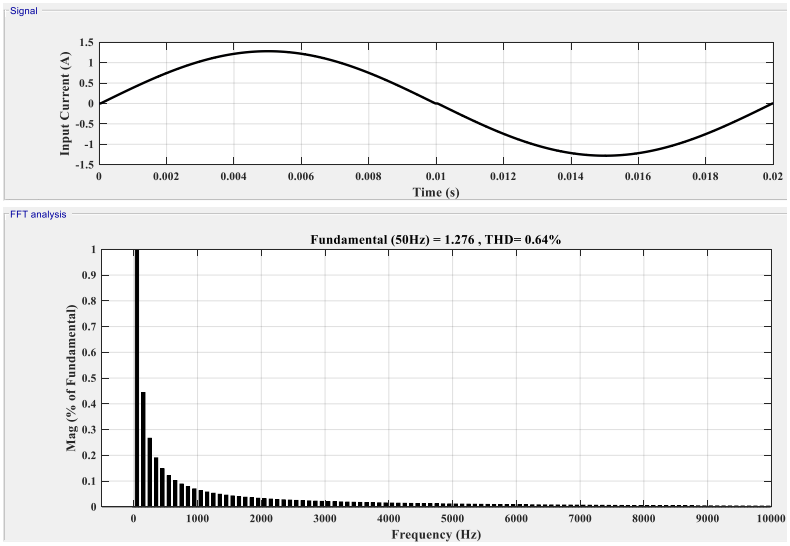


Figure 8. Power quality analysis of the input current.

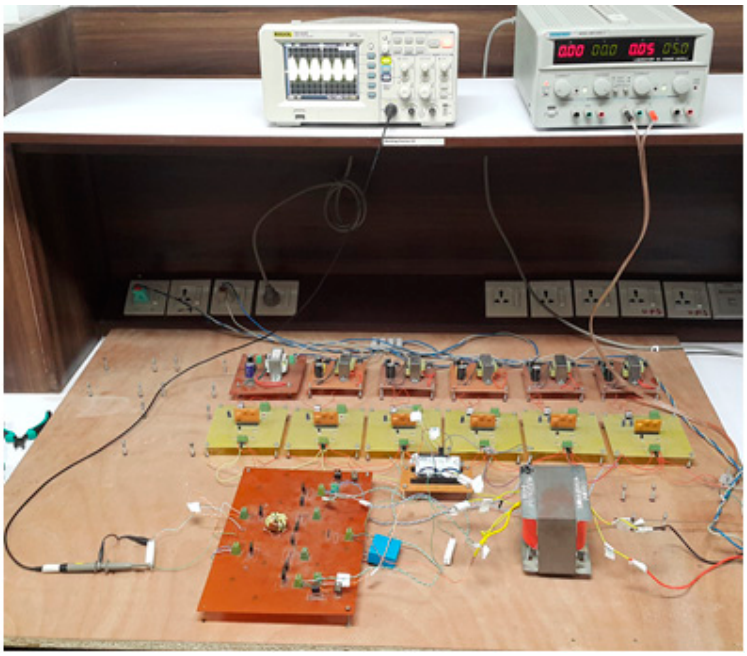


Figure 9. Practical setup.

A capacitor of 1 μF is used at the source side to suppress the unwanted harmonics generated by the high-frequency switches. An intermediate inductor of 1 mH is employed to solve the shoot-through problem caused by the complementary switching of the controlled devices. To explore the operation without zero-crossing detection, the analysis of the proposed topology is carried out by generating the required control signals with ZCD and without ZCD. For this purpose, the output frequency is selected 400 Hz so that the output voltage waveforms with their FFT can be clearly viewed. Figures 10 and 11 show the practically recorded waveforms for 400 Hz output frequency with ZCD and without ZCD, respectively. The 400 Hz output frequency is generated by non-inverting and inverting the input voltage eight times during one cycle, as can be seen in Figures 10 and 11. All the practical waveforms are recorded with the Rigol oscilloscope.

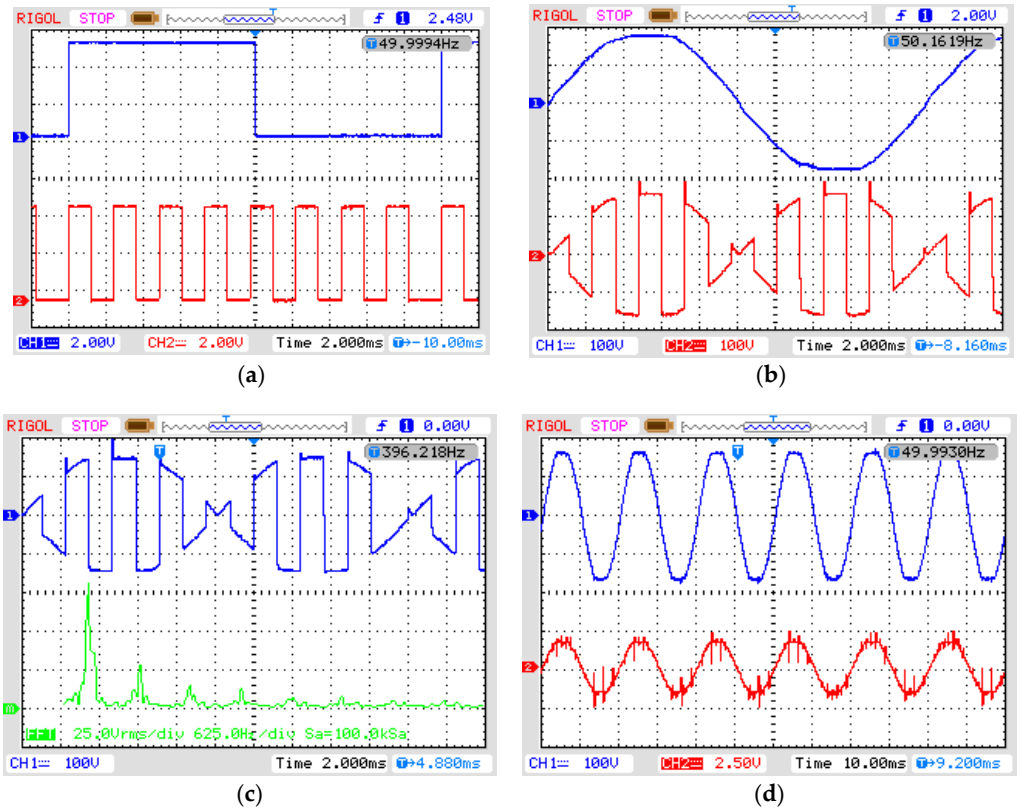


Figure 10. Outputs with zero-crossing detector (ZCD): (**a**) switching signals; (**b**) input-output voltage waveform; (**c**) fast Fourier transform (FFT) of the output voltage waveform; (**d**) input voltage-current waveforms.

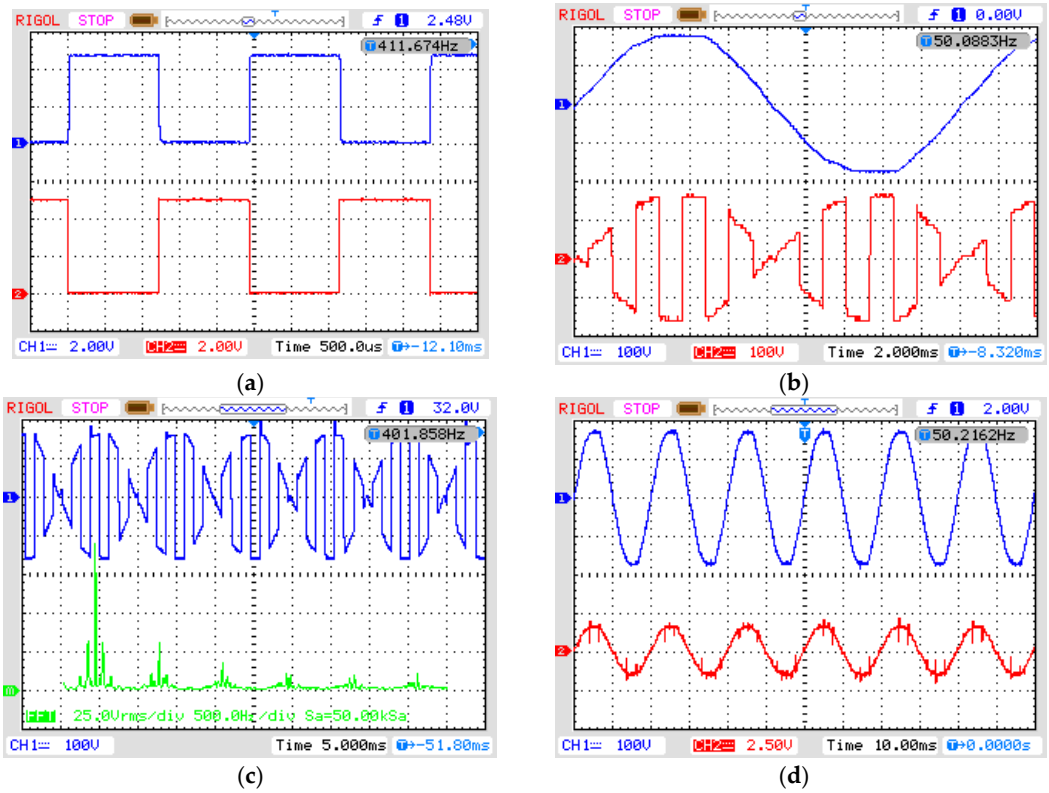
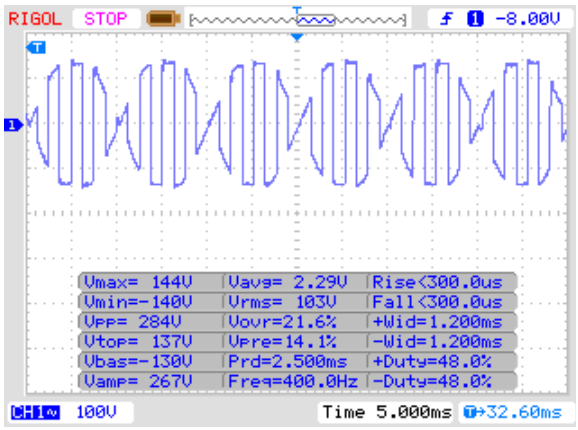


Figure 11. *Cont.*



(**e**)

Figure 11. Outputs without ZCD: (**a**) switching signals; (**b**) input-output voltage waveforms; (**c**) FFT of the output voltage; (**d**) input voltage-current waveforms; (**e**) rms value of the output voltage.

Figure 10a depicts the switching signal generated with ZCD so that it may be synchronized with the input voltage. It is generated by applying an interrupt to the Arduino once ZCD detects the positive zero crossings. In Figure 10b, the output voltage is plotted with respect to the input voltage, while Figure 10c determines the harmonics contents of the output voltage, where the dominant component exists at 400 Hz. The analysis of these figures depicts that the period of the output voltage is eight times lesser than that of the input voltage. Therefore, the output frequency is eight times greater than the frequency of the source voltage. Figure 10d presents the input current waveform with respect to the input voltage. The input current is nearly sinusoidal, ensuring low harmonic contents and low THD. This ensures improvement in the input power factor.

Figure 11a depicts the practically recorded waveforms of two complementary switching signals generated without zero-crossing detection. So, they are not synchronized with the input voltage. They are simply generated without any zero-crossing interrupt with any PWM generator. This characteristic simplifies the control effort significantly and reduces its complexity for the induction heating application. The analysis of Figure 11b–d determines the power quality of the output voltage and input current. The rms value of the output voltage is recorded in Figure 11e. This also validates the computed rms value of Equation (13) in Section 1. The comparison of Figures 10 and 11 depicts that the power quality characteristics of the output voltage and input current with and without zero-crossing detection are almost similar. This is true if output frequency is a few hundred times greater than that of the frequency of the source voltage. So, switching sequences can be directly generated and applied to the controlled switches. That is why the proposed topology is implemented without zero crossing detection for the induction heating application.

The nominal output frequency requirement in the domestic induction heating application lies in the range of 20 kHz to 100 kHz. The switching frequency of the converter is selected higher than the resonance frequency, so the effect of load equivalent inductance and capacitance should not reflect in the output and input currents. The resonance of the equivalent load inductance (40 µH), filtering inductor (1 mH), capacitance (1 µF), and resistance (120 Ω) is nearly 5 kHz. The switching sequence of 25 kHz is applied to the switching devices to obtain the output frequency of 25 kHz. This is achieved by operating the proposed converter 500 times in non-inverting and inverting modes in one cycle of the input voltage. That is why the output and input currents are in-phase with their corresponding voltage ensuring improved power quality.

Figure 12a shows the two complementary gating signals for 25 kHz switching frequency. Figure 12b,c depicts the output voltage and current waveforms. The power quality of the input current is explored by plotting it with respect to the input voltage in Figure 12d.

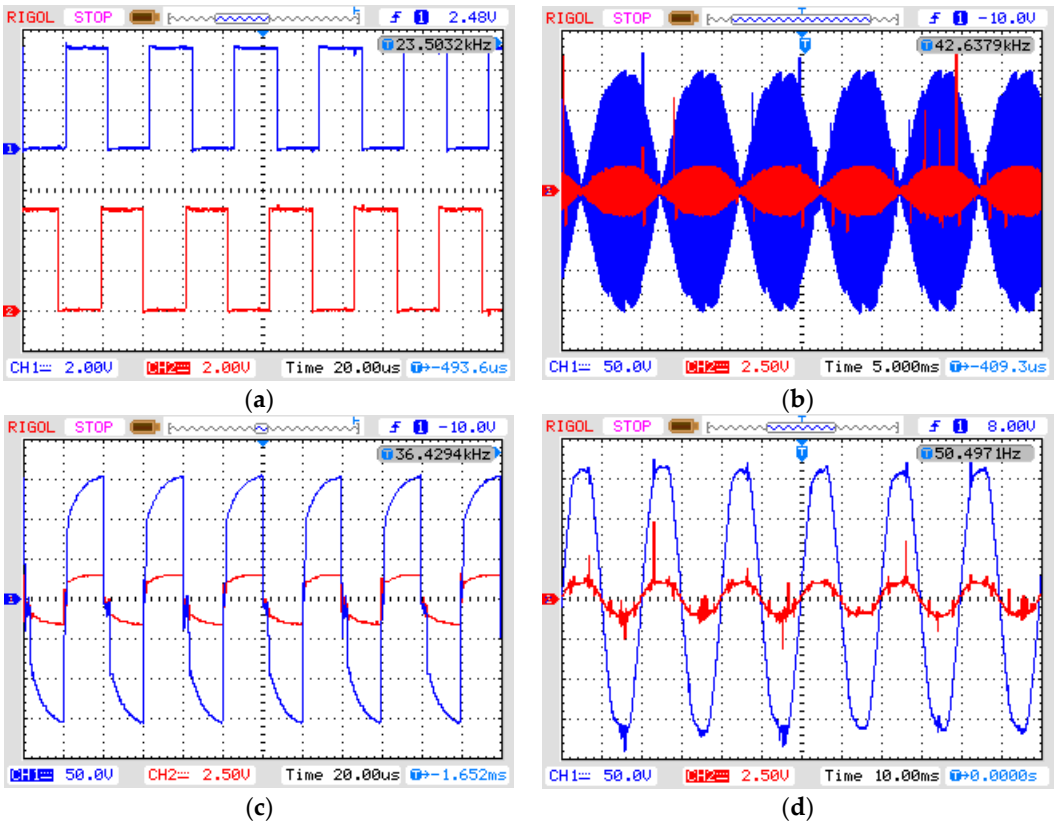


Figure 12. Outputs with 25 kHz switching frequency: (**a**) switching signals; (**b**) output voltage-current waveforms; (**c**) output voltage-current waveforms in zoom form; (**d**) input voltage-current waveforms.

The envelope of the output voltage of Figure 12b is equal and opposite to the instantaneous value of the input voltage. Figure 12c is obtained by zooming the Figure 12b around the peak value (150 V) of the input voltage to explore that the instantaneous value of the output voltage is equal to 150 V during non-inverting and −150 V during the inverting operation for positive input voltage. However, the rms values of the output and the input voltage are the same.

All the practically recorded waveforms of input currents (see Figures 10–12) have the same sinusoidal behavior ensuring low harmonic contents, low THD, and hence improved power factor. There is no voltage and current overshoot problem in output voltage, output, and input current. These characteristics of the proposed converter make it very attractive for the induction heating application.

5. Conclusions

This research work proposed a novel single-phase direct frequency converter for domestic induction heating application. The required high-frequency ac output is directly obtained from the low-frequency input voltage with a simple control algorithm. The switching sequences are directly generated from any simple low-cost PWM generator as there is no need to detect the positive or negative half cycle of the input voltage. The developed converter is implemented with only six controlled switching devices and six fast recovery diodes. Therefore, this development of the proposed converter reduces the size and cost by eliminating the requirements of two extra controlled switches, two fast recovery diode, two gate-drive circuits, two isolated dc power supplies, and one zero-crossing detector as compared to the existing converters. The proposed converter is also immune from a shoot-through problem caused by the complementary switching of the controlled devices. The proposed topology is first implemented in the MATLAB/Simulink environment then validated by the practical results obtained by developing a hardware setup.

Author Contributions: Conceptualization, N.A. and G.A.; data curation, A.B.A.; formal analysis, T.I., G.A. and V.E.B.; investigation, U.F.; methodology, N.A., G.A., A.B.A., A.S.A. and A.G.A.; resources, A.S.A. and K.S.; supervision, T.I.; validation, V.E.B.; visualization, U.F.; writing—original draft, N.A. and G.A.; writing—review and editing, A.B.A., A.S.A., A.G.A.-K., and K.S. All authors have read and agreed to the published version of the manuscript.

Funding: This research work is supported by the Deanship of Scientific Research, Majmaah University under contract number RGP-2019-19 and the University of Engineering and Technology, Lahore, Pakistan.

Acknowledgments: The authors extend their appreciation to the Deanship of Scientific Research, Majmaah University for funding this work under project number No (RGP-2019-19). The authors would like to express their gratitude to University of Engineering and Technology for the administrative and technical support.

Conflicts of Interest: The authors declare no conflict of interest.

References

1. Sarnago, H.; Lucía, O.; Burdio, J.M. Multiresonant Power Converter for Improved Dual-Frequency Induction Heating. *IEEE Trans. Power Electron.* **2019**, *34*, 2097–2103. [CrossRef]
2. Acero, J.; Burdio, J.M.; Barragan, L.A.; Navarro, D.; Alonso, R.; Ramon, J.; Monterde, F.; Hernandez, P.; Llorente, S.; Garde, I. Domestic Induction Appliances. *IEEE Ind. Appl. Mag.* **2010**, *16*, 39–47. [CrossRef]
3. Sarnago, H.; Lucia, O.; Mediano, A.; Burdio, J.M. Modulation Scheme for Improved Operation of an RB-IGBT-Based Resonant Inverter Applied to Domestic Induction Heating. *IEEE Trans. Ind. Electron.* **2013**, *60*, 2066–2073. [CrossRef]
4. Sarnago, H.; Lucía, Ó.; Mediano, A.; Burdío, J.M. Class-D/DE Dual-Mode-Operation Resonant Converter for Improved-Efficiency Domestic Induction Heating System. *IEEE Trans. Power Electron.* **2013**, *28*, 1274–1285. [CrossRef]
5. Di Barba, P.; Dughiero, F.; Sieni, E.; Candeo, A. Coupled Field Synthesis in Magnetic Fluid Hyperthermia. *IEEE Trans. Magn.* **2011**, *47*, 914–917. [CrossRef]
6. Shin, S.; Shin, J.; Song, B.; Lee, S.; Kim, Y.; Jung, G.; Jeon, S. Wireless power transfer system for high power application and a method of segmentation. In Proceedings of the 2013 IEEE Wireless Power Transfer (WPT), Perugia, Italy, 15–16 May 2013; pp. 76–78.
7. Da Silva Filho, O.C.; de Almeida, B.R.; de Souza Oliveira Júnior, D.; Fernandes Neto, T.R. High-Frequency Isolated AC–DC–AC Interleaved Converter for Power Quality Applications. *IEEE Trans. Ind. Appl.* **2018**, *54*, 4594–4602. [CrossRef]
8. Rodrigues, P.L.S.; Jacobina, C.B.; de Rossiter Corrêa, M.B.; da Silva, I.R.F.M.P. Single-Phase Universal Active Power Filter Based on Four-Leg AC–DC–AC Converters. *IEEE Trans. Ind. Appl.* **2019**, *55*, 1639–1648. [CrossRef]
9. Ashraf, N.; Izhar, T.; Abbas, G. A Single-Phase Buck-Boost Matrix Converter with Low Switching Stresses. *Math. Probl. Eng.* **2019**, *2019*, 6893546. [CrossRef]
10. Ashraf, N.; Izhar, T.; Abbas, G.; Balas, V.E.; Balas, M.M.; Lin, T.-C.; Asad, M.U.; Farooq, U.; Gu, J. A Single-Phase Buck and Boost AC-to-AC Converter with Bipolar Voltage Gain: Analysis, Design, and Implementation. *Energies* **2019**, *12*, 1376. [CrossRef]
11. Khan, U.A.; Khan, A.A.; Cha, H.; Kim, H.G.; Kim, J.; Baek, J.W. Dual Buck AC-AC Converter with Inverting and Non-Inverting Operations. *IEEE Trans. Power Electron.* **2018**, *33*, 9432–9443. [CrossRef]
12. Nazarpour, D.; Farzinnia, M.; Nouhi, H. Transformer-less dynamic voltage restorer based on buck-boost converter. *IET Power Electron.* **2017**, *10*, 1767–1777. [CrossRef]
13. Zhou, M.; Sun, Y.; Su, M.; Li, X.; Lin, J.; Liang, J.; Liu, Y. Transformer-less dynamic voltage restorer based on a three-leg ac/ac converter. *IET Power Electron.* **2018**, *11*, 2045–2052. [CrossRef]
14. Huang, J.; Zhang, A.; Zhang, H.; Ren, Z.; Wang, J.; Zhang, L.; Zhang, C. Improved Direct Power Control for Rectifier Based on Fuzzy Sliding Mode. *IEEE Trans. Control Syst. Technol.* **2014**, *22*, 1174–1180. [CrossRef]
15. Sarnago, H.; Lucía, O.; Burdio, J.M. A Versatile Resonant Tank Identification Methodology for Induction Heating Systems. *IEEE Trans. Power Electron.* **2018**, *33*, 1897–1901. [CrossRef]
16. Park, H.; Jung, J. Load-Adaptive Modulation of a Series-Resonant Inverter for All-Metal Induction Heating Applications. *IEEE Trans. Ind. Electron.* **2018**, *65*, 6983–6993. [CrossRef]
17. Villa, J.; Artigas, J.I.; Beltran, J.R.; Vicente, A.D.; Barragan, L.A. Analysis of acoustic noise spectrum of domestic induction heating systems controlled by phase-accumulator modulators. *IEEE Trans. Ind. Electron.* **2019**, *66*, 5929–5938. [CrossRef]

18. Ursaru, O.; Lucanu, M.; Aghion, C.; Lucanu, N. Single-Phase Direct Boost AC-AC Converter. *Adv. Electr. Comput. Eng.* **2017**, *17*, 43–49. [CrossRef]
19. Li, P.; Hu, Y. Unified Non-Inverting and Inverting PWM AC–AC Converter with Versatile Modes of Operation. *IEEE Trans. Ind. Electron.* **2017**, *64*, 1137–1147. [CrossRef]
20. Ahmed, H.F.; Cha, H.; Khan, A.A.; Kim, H.G. A Novel Buck–Boost AC–AC Converter with both Inverting and Noninverting Operations and Without Commutation Problem. *IEEE Trans. Power Electron.* **2016**, *31*, 4241–4251. [CrossRef]
21. Zhou, M.; Sun, Y.; Su, M.; Li, X.; Liu, F.; Liu, Y. A single-phase buck-boost AC-AC converter with three legs. *J. Electr. Eng. Technol.* **2018**, *13*, 838–848.
22. Liu, C.; Guo, D.; Shan, R.; Cai, G.; Ge, W.; Huang, Z.; Wang, Y.; Zhang, H.; Wang, P. Novel Bipolar-Type Direct AC-AC Converter Topology based on Non-Differential AC Choppers. *IEEE Trans. Power Electron.* **2019**, *34*, 9585–9599. [CrossRef]
23. Ahmed, H.F.; Cha, H.; Khan, A.A.; Kim, J.; Cho, J. A Single-Phase Buck–Boost Matrix Converter with only Six Switches and Without Commutation Problem. *IEEE Trans. Power Electron.* **2016**, *32*, 1232–1244. [CrossRef]
24. Zhou, M.; Sun, Y.; Su, M.; Li, X.; Liu, F.; Liu, Y. A Single-phase Buck-boost AC-AC Converter with Three Legs. *J. Electr. Eng. Technol.* **2018**, *13*, 838–848.
25. Ashraf, N.; Izhar, T.; Abbas, G. An efficient single-phase ac-to-ac buck and boost matrix converter. In Proceedings of the 2017 International Conference on Electrical Engineering (ICEE), Lahore, Pakistan, 2–4 March 2017; pp. 1–5.
26. Song, W.; Liu, J.; Sun, X.; Wu, F.; Gao, D.; Wang, Y. Research on Commutation and Coordination Control Strategy of Excitation Power Supply Based on Bidirectional Reduced Matrix Converter for Ion Accelerator. *Energies* **2018**, *11*, 3396. [CrossRef]
27. Kumar, A.; Kumar Sadhu, P.; Kumar Mohanta, D.; Bharata Reddy, M. An Effective Switching Algorithm for Single Phase Matrix Converter in Induction Heating Applications. *Electronics* **2018**, *7*, 149. [CrossRef]
28. Jung, H.Y.; Kim, S.H.; Moon, B.; Lee, S.-H. A new circuit design of two-switch buck-boost converter. *IEEE Access* **2018**, *6*, 47415–47423. [CrossRef]
29. Nguyen, M.-K.; Jung, Y.-G.; Lim, Y.-C.; Kim, Y.-M. A single-phase Z-source buck–boost matrix converter. *IEEE Trans. Power Electron.* **2009**, *25*, 453–462. [CrossRef]



© 2020 by the authors. Licensee MDPI, Basel, Switzerland. This article is an open access article distributed under the terms and conditions of the Creative Commons Attribution (CC BY) license (http://creativecommons.org/licenses/by/4.0/).